Electronic Supplementary Material (ESI) for Physical Chemistry Chemical Physics.

Self-assembly of polyelectrolyte diblock copolymers within mixtures of monovalent and multivalent counterions

Li-Yan Liu[a], Zhong-Xun Yu[b], Li-Xiang Liu[a], Jing-Qi Yang[c], Qing-Hai Hao[a], Tong Wei[a], Hong-Ge Tan[a]

[a] College of Science, Civil Aviation University of China

[b] School of Materials Science and Engineering, Beijing University of Chemical Technology

[c] College of Flight Technology, Civil Aviation University of China

Supporting Information

Simulation Details

van der Waals interactions between any two individual beads are described by a shifted and truncated Lennard-Jones (LJ) potential,

$$U_{LJ}(r_{ij}) = \begin{cases} 4\varepsilon_{LJ}\left[\left(\frac{\sigma}{r_{ij}}\right)^{12} - \left(\frac{\sigma}{r_{ij}}\right)^{6} - \left(\frac{\sigma}{r_c}\right)^{12} + \left(\frac{\sigma}{r_c}\right)^{6}\right] & r_{ij} < r_c \\ 0 & r_{ij} > r_c \end{cases} \quad (1)$$

where r_{ij} represents the distance between any two beads, ε_{LJ} defines the strength of pairwise interaction, σ is the bead diameter which is selected to be the same regardless of the bead type, and r_c is the cutoff radius. The hydrophobicity of B-block is presented by the interactions between hydrophobic beads.

Bonded interactions between adjacent monomers along the copolymer chain are treated with a finitely extensible nonlinear elastic (FENE) potential:

$$U_{bond}(r_{ij}) = -\frac{1}{2}kR^2{}_0 \ln\left[1 - \left(\frac{r_{ij}}{R_0}\right)^2\right] \quad (2)$$

The commonly accepted values for the constants are used, $k=30k_BT/\sigma$ and $R_0=1.5\sigma$. k and R_0 are the spring constant and the maximum bond length, respectively.

The motion of all beads is described by the Langevin equation:

$$m\frac{d^2\vec{r}_i(t)}{dt^2} = -\nabla U_i - \xi\frac{d\vec{r}_i(t)}{dt} + \vec{F}_i^R(t) \tag{3}$$

where m is the bead mass, which is the same regardless of bead type; U_i is the total potential of the system; ξ is the friction coefficient, $\xi = 1.0m\tau^{-1}$, where τ is the standard LJ time unit, $\tau = \sigma(m/\varepsilon_{LJ})^{1/2}$. The random force $\vec{F}_i^R(t)$ has zero average value, $\langle \vec{F}_i^R(t) \rangle = 0$, and δ-functional correlations $\langle \vec{F}_i^R(t)\vec{F}_i^R(t') \rangle = 6k_BT\xi\delta(t-t')$. The motion of beads was generated using the velocity Verlet algorithm, a time step of $\Delta t = 0.005\tau$ was applied for integration of the equations of motion (eq. (4)). To make the self-assembly structures independent of the initial configuration, the copolymers and counterions are distributed randomly in the simulation box at the start of the simulation.

Micellar evolution

The average aggregation number of micelles as a function of time in the mixture of monovalent and divalent ions is shown in Fig. 1.

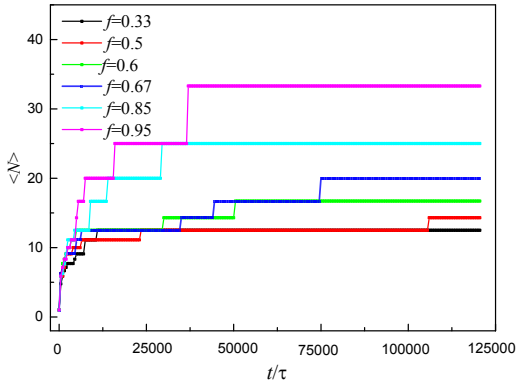

Fig. 1. The average aggregation number of micelles as a function of time in the mixture of monovalent and divalent ions.

Fig. 2 depicts the fusion process at f_{3c}=0.67.

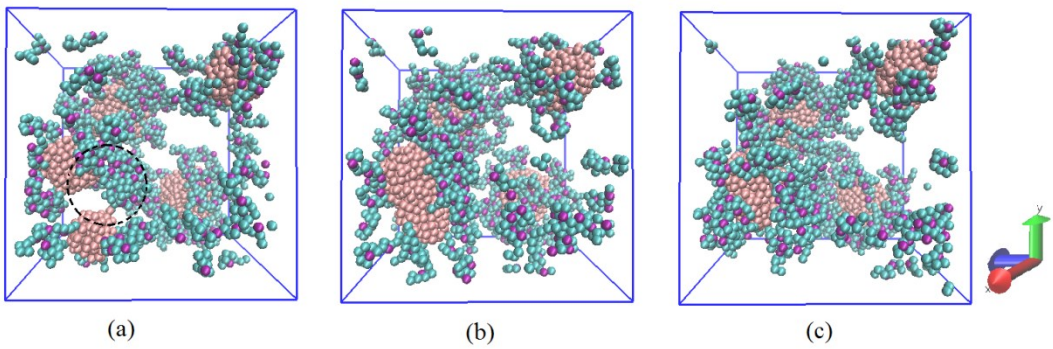

Fig. 2. The snapshots display the micellar fusion process at f_{3c}=0.67, where cyan bead represents the hydrophilic monomer, and purple for trivalent ion.

Fig. 3 displays micellar fission and reequilibration at f_{3c}=0.95 when the temperature of the system jumps to a higher value $T = 3.0\varepsilon_{LJ}/k_B$.

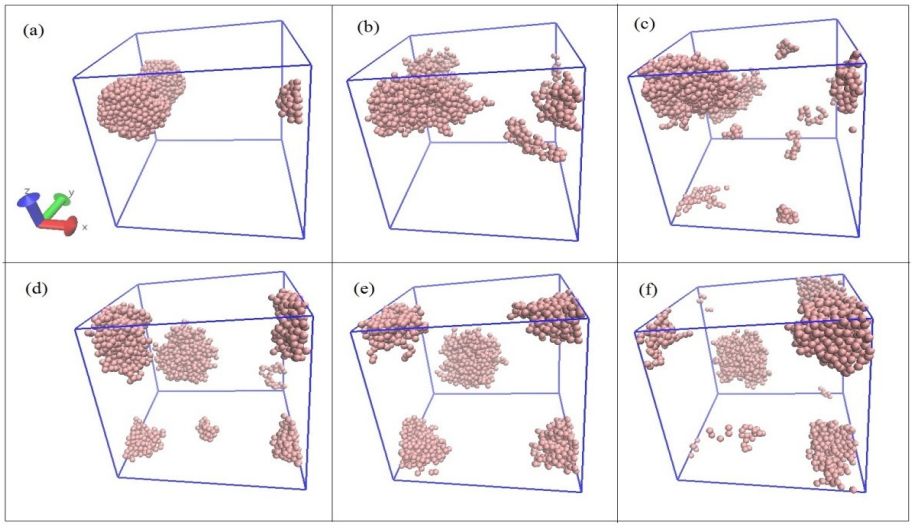

Fig. 3. The snapshots display the reequilibrated process at f_{3c}=0.95 when the temperature of the system jumps to $T = 3.0\varepsilon_{LJ}/k_B$. The equilibrated configuration at $T = 1.0\varepsilon_{LJ}/k_B$ is set as the original state (a).

The verification of the presentation of FCC structure after translating the coordinate origin of the simulation box to the center of mass of the second micelle

To quantitatively verify the FCC structure, two features should be demonstrated. First, the other three micelles should be proven to stay on the planes composed of the centers of mass of the second micelle. Using the *y*–*z* plane in Fig. 4(b) as an example, in the ideal case, the center of mass of the first micelle should be on the *y*–*z* plane, namely, have the same *x*-coordinate as the plane. If not, the *x*-coordinate of the plane

should be between the maximum and minimum coordinate of the first micelle in the *x*-direction. Similarly, the *x*–*z* and *x*–*y* planes should be between the maximum and minimum coordinates of the third and fourth micelles in the *y*- and *z*-directions, respectively. Second, the micelles should be on the centers of the planes, and the centroid distance between the second and other micelles should be $\sqrt{2}L\sigma/2$. In this study, as L=33σ, then the standard centroid distance is 23.3σ. Fig. 5 shows changes in the center of mass of the first and second, second and third, and second and fourth micelles, and the maximum and minimum coordinates of the first, third, and fourth micelles in the *x*-, *y*-, and *z*-directions with respect to time, with their averages shown in Figs. 5(a), 5(b), and 5(c), respectively. These results show that the other three micelles almost always remain on the planes composed of the centers of mass of the second micelle, with the average values implying that the planes pass through the corresponding micelles almost symmetrically. The centroid distances between the second and other micelles are shown in Fig. 5(d). The average centroid distances between the second and first, and third and fourth micelles are 24.6σ, 22.5σ, and 21.0σ, and the relative deviations were 5.4%, 3.6%, and 9.9%, respectively.

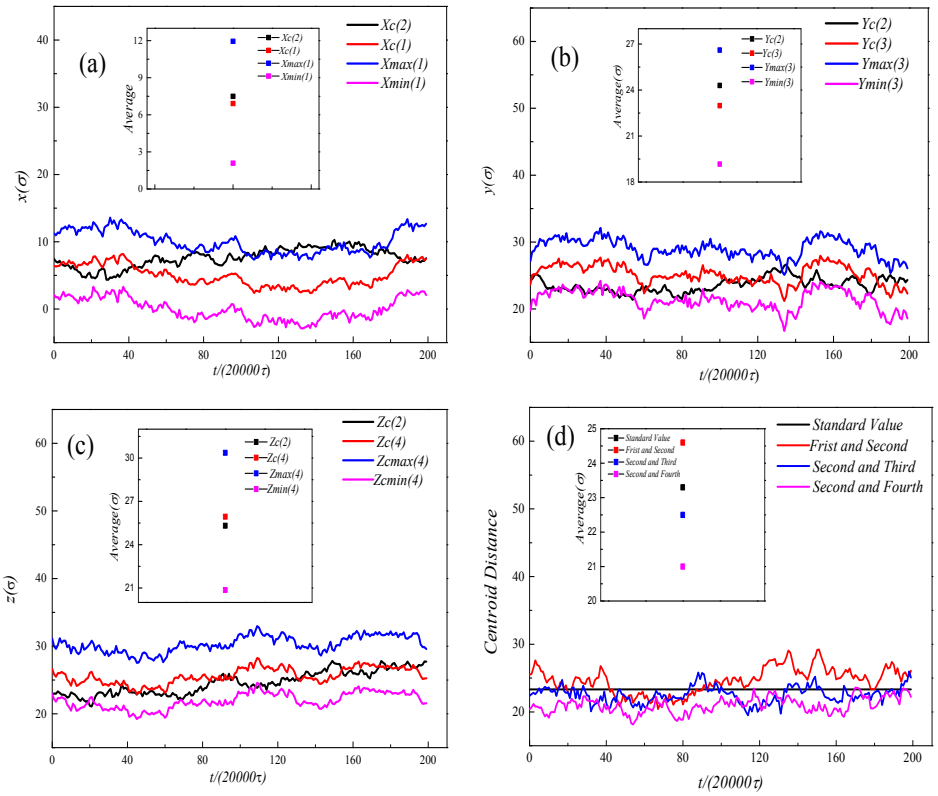

Fig. 4. The changes of the centroid coordinates of the first and second, the second and third, the second and forth micelle, and the maximum, minimum coordinate of the first, third and forth micelle in x-, y- and z-direction with respect to time and their averages are showed in (a), (b) and (c), respectively. In (d), the changes of the centroid distances between the second and others micelles with respect to time and their averages are displayed.

Top-down view of polymer monomers and counterion density profiles on the *x*–*y* plane

Fig.5. depicts the density profiles of polymer monomers and counterions on *x*-*y* plane in the mixture of monovalent and divalent ions.

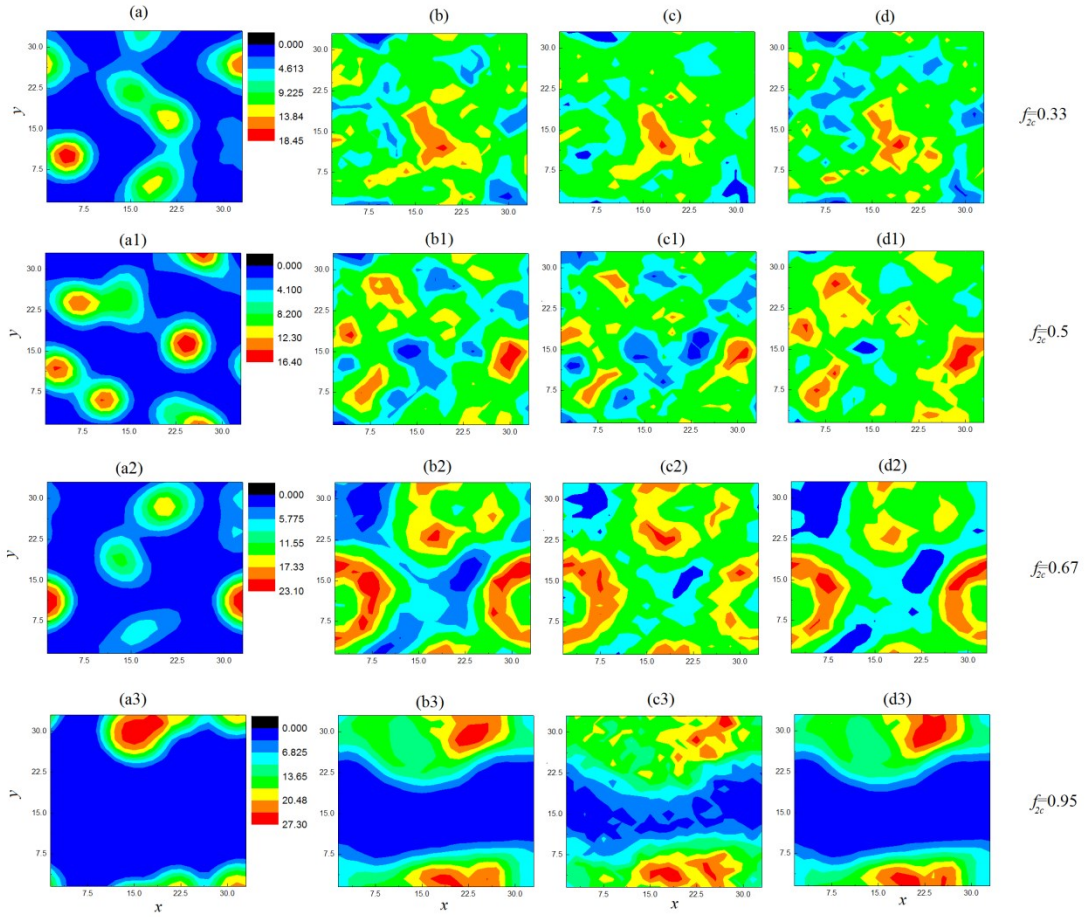

Fig.5. Time-averaged top-down view of polymer monomers and counterion density profiles on x–y plane in the mixture of monovalent and divalent ions. Profiles of hydrophobic monomers, hydrophilic monomers, monovalent ions, and trivalent ions are shown in first, second, third and fourth columns, respectively.

Fig.6. displays the density profiles of polymer monomers and counterions on x-z and y-z planes at f_{3c}=0.95.

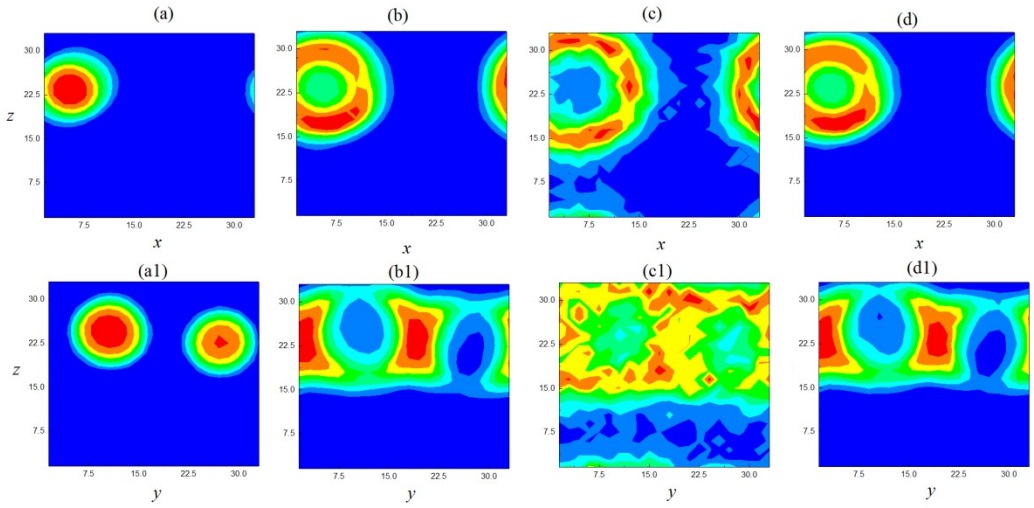

Fig. 6. Top-down views of hydrophobic monomer (first column), PE monomer (second column), monovalent ions (third column),and multivalent ions (fourth column) density profiles on x–z, and y–z planes at f_{3c}=0.95.

Fig.7 shows the schematic picture for the average number of absorbed PE monomers per multivalent ion.

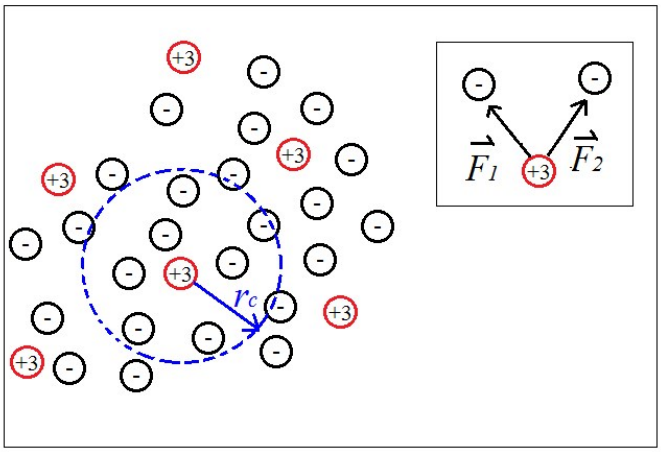

Fig. 7. Schematic picture for the average number of absorbed monomers per trivalent ion.